Chemical Science

ROYAL SOCIETY OF CHEMISTRY

EDGE ARTICLE

View Article Online
View Journal | View Issue

Cite this: *Chem. Sci.*, 2021, **12**, 4094

All publication charges for this article have been paid for by the Royal Society of Chemistry

On the location of Lewis acidic aluminum in zeolite mordenite and the role of framework-associated aluminum in mediating the switch between Brønsted and Lewis acidity†

Manoj Ravi, [a] Vitaly L. Sushkevich [b] and Jeroen A. van Bokhoven *[ab]

Received 6th November 2020
Accepted 25th January 2021

DOI: 10.1039/d0sc06130a

rsc.li/chemical-science

Lewis acidic aluminum in zeolites, particularly acidity that is inherent to the framework, is an indeterminate concept. A fraction of framework aluminum changes geometry to octahedral coordination in the proton form of zeolite mordenite. Such octahedrally coordinated aluminum is the precursor of a Lewis acid site and its formation is accompanied by a loss in Brønsted acidity. Herein, we show that such Lewis acid sites have a preferred location in the pore structure of mordenite. A greater proportion of these Lewis acid sites resides in the side-pockets than in the main channel. By reverting the octahedrally coordinated aluminum back to a tetrahedral geometry, the corresponding Brønsted acid sites are restored with a concomitant loss in the ability to form Lewis acid sites. Thereby, reversible octahedral–tetrahedral aluminum coordination provides a means to indirectly switch between Lewis and Brønsted acidity. This phenomenon is unique to Lewis acidity that is inherent to the framework, thereby distinguishing it from Lewis acidity originating from extra-framework species. Furthermore, the transformation of framework aluminum into octahedral coordination is decoupled from the generation of distorted tetrahedrally coordinated aluminum, where the latter gives rise to the IR band at 3660 cm^{-1} in the OH stretching region.

Introduction

Zeolites are extensively used as catalyst and support materials for a wide array of industrially applied reactions.[1,2] The presence of tetrahedrally coordinated aluminum in a zeolite framework necessitates a charge-compensating cation to yield a neutral material. When this cation is a proton, it results in a Brønsted acid site (Fig. 1a),[3] which is at the origin of industrial application of zeolites as solid acid catalysts, replacing homogeneous mineral acids in various processes.[4] Protonic zeolites are extensively used for several reactions, in particular, cracking, alkylation, and isomerization.[5–7] Apart from Brønsted acid sites, certain aluminum species in zeolites possess Lewis acidic character. Lewis acidic aluminum (Fig. 1b) plays a pivotal role not only in traditional cracking reactions, but also in salient biomass valorization reactions,[8,9] which include the conversion of trioses to alkyl lactates,[10] and cellulose to glucose.[11] Conventionally, one of the oft-used techniques to study the above-mentioned acid sites in zeolites is FTIR spectroscopy of adsorbed probe molecules.[12,13] Not only can Lewis acid sites be distinguished easily from Brønsted acid ones, but finer nuances, such as acid site strength and accessibility can also be assessed. For instance, evacuating adsorbed pyridine at different temperatures provides information on the strength of adsorption, which to some extent relates to acid site strength.[14–16] Likewise, using probe molecules of different sizes sheds light on the accessibility of the sites.[17]

Alongside Lewis acidic aluminum species in zeolites, Brønsted acid sites engage in a cooperative fashion to catalyze multi-step 'domino' reactions.[18] Examples of such reactions in biomass valorization chemistry include the conversion of glucose to 5-hydroxymethylfurfural (HMF) and of C_3-sugars to lactic acid esters.[19–21] These conversions feature consecutive reaction steps that take place over different active sites and consequently, require a precise balancing of the number of Lewis and Brønsted acid sites in the zeolite. This is

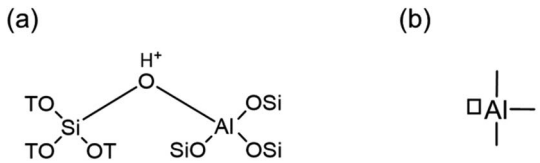

Fig. 1 Sketch of (a) Brønsted acid site and (b) three-coordinated Lewis acid site in a zeolite.

[a]*Institute for Chemical and Bioengineering, Department of Chemistry and Applied Biosciences, ETH Zurich, 8093 Zurich, Switzerland. E-mail: jeroen.vanbokhoven@chem.ethz.ch*

[b]*Laboratory for Catalysis and Sustainable Chemistry, Paul Scherrer Institute, Villigen, 5232, Switzerland*

† Electronic supplementary information (ESI) available. See DOI: 10.1039/d0sc06130a

experimentally evident from the existence of an optimal Lewis to Brønsted acid ratio to achieve the highest yield of the product.[20,21] Likewise, in glycerol dehydration over zeolites, Brønsted acid sites are involved in activating the substrate, but the selectivity to acrolein or acetaldehyde is dictated by the Lewis acid content in the zeolite.[22] Consequently, understanding the skew of these two different types of acid sites is paramount for the catalytic applications of zeolites. However, despite zeolites being used commercially on a large scale and extensive research being carried out over a number of decades now, the origin of Lewis acidity in these materials remains a nebulous concept.[15,23–30] Several proposals for Lewis acidic aluminum species exist, which include framework aluminum,[26,27,31] extra-framework aluminum (EFAl),[25,32–34] and framework-associated aluminum.[15,30] In a recently published perspective, we discussed this classification in detail and illustrated that the multiple proposals point towards a plurality of Lewis acid sites and mechanisms that generate these species.[35] The uncertainty in demarcating the origin of Lewis acidic aluminum in zeolites hampers the analysis of Lewis–Brønsted acid synergy in catalytic applications.[36,37]

The most extensively characterized mechanism for Lewis acidity in zeolites is of that formed after dealumination *via* steaming.[38] This route entails the hydrolysis of framework Si–O–Al bonds, translating in the removal of aluminum from the framework.[32,34,39–42] In comparison to this mechanism, the proposal of Lewis acidity that is inherent to the zeolite framework is less rigorously examined, but has received greater attention of late.[26,35,43,44] NMR experiments performed at high fields have enabled the characterization of a second framework Al(IV) site,[45] and the elucidation of the acidic nature of tri-coordinated framework aluminum in dehydrated ZSM-5.[43] The precursor to Lewis acid sites in this mechanism – unlike for the Lewis acid sites generated from EFAl – is tetrahedral framework aluminum.

Framework-associated aluminum refers to species that can undergo reversible changes in coordination from octahedral to tetrahedral.[46] Through a combination of ^{27}Al MAS NMR and FTIR spectroscopy, we demonstrated that framework-associated aluminum can be assigned Lewis acidic property in zeolite mordenite.[30] It adopts an octahedral coordination in the proton form of the zeolite after calcination in static air and exposure of the sample to moisture under ambient conditions.[15,30,46,47] Such an aluminum species is associated with Lewis acidity upon dehydration.[30,48] The octahedrally coordinated framework-associated species can be reverted into a normal framework tetrahedral coordination, and should therefore, not be described as simply extra-framework. While the Lewis acidic character of framework-associated aluminum was evidenced, the nature of these species, its evolution as a function of conditions, and its location in the pore system of zeolite mordenite remain unaddressed. Also, the potential role of distorted tetrahedral and penta-coordinated aluminum in generating Lewis acidity was not evaluated. As per current knowledge, the extent to which the generation of these latter species are coupled to the generation of framework-associated octahedrally coordinated aluminum is unknown. By targeting these knowledge gaps, our objective is to arrive at a better understanding of the Lewis acidic property of framework-associated aluminum and of zeolites in general. We demonstrate how evolution in aluminum coordination with varying conditions influences both Lewis and Brønsted acidity in the zeolite, with the two kind of acid sites being partially interchangeable. Furthermore, we highlight the role of the side-pockets in mordenite in this phenomenon. Current knowledge on the generation of Lewis acid sites, irrespective of which kind of aluminum species shows Lewis acidic property, is that they are formed with a loss in Brønsted acidity.[24,26,49] Overall, we report a novel conceptual advance on the possibility to toggle between Lewis and Brønsted acidity, founded on the basis of aluminum species that exhibit reversible octahedral–tetrahedral coordination. The Lewis acid sites generated from such aluminum species are preferentially located in the side-pockets as opposed to the main channel of mordenite.

Results and discussion

Aluminum structure from ^{27}Al MAS NMR

Fig. 2 illustrates that the coordination of aluminum in zeolite MOR is a function of the charge-compensating cation and treatment conditions, in line with what is typically observed for zeolites.[46,47,50] The details of sample nomenclature and treatment procedure are provided in Table 1. Since the aluminum structure is sensitive to many factors, such as water content and temperature,[48,51] the structure determined by a conventional ^{27}Al MAS NMR experiment is the structure that prevails after

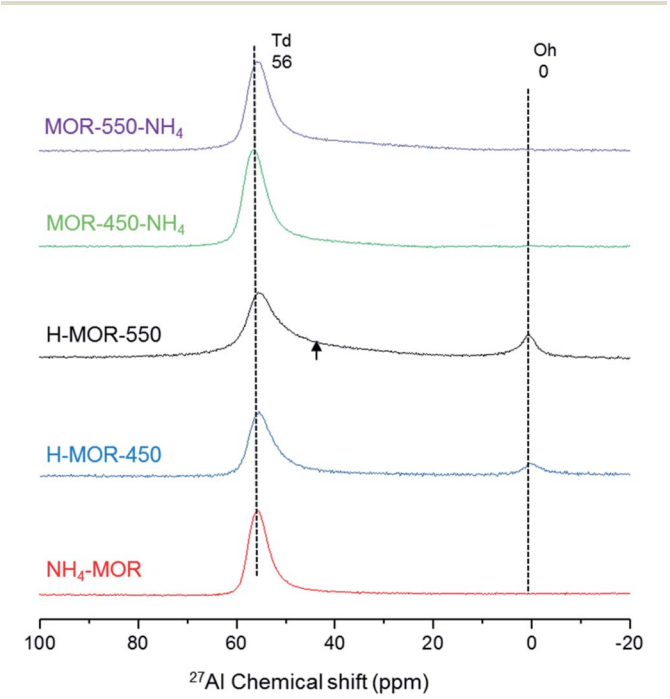

Fig. 2 ^{27}Al MAS NMR spectra of zeolite MOR under ambient conditions of NH_4–MOR, H–MOR-450, H–MOR-550, MOR-450-NH_4 and MOR-550-NH_4. The broad shoulder at the high field side of the peak corresponding to tetrahedrally coordinated framework aluminum in H–MOR-550 is highlighted by the black arrow mark.

Table 1 Sample name and treatment procedure. A more detailed description of synthesis procedures is provided in the experimental section in the ESI

Sample name	Treatment procedure
NH_4–MOR	Commercial mordenite zeolite in the ammonium form, Zeolyst CBV21A, Si/Al = 11
H–MOR-450	NH_4–MOR calcined at 450 °C in static air & subsequent exposure to ambient conditions
H–MOR-550	NH_4–MOR calcined at 550 °C in static air & subsequent exposure to ambient conditions
MOR-450-NH_4	H–MOR-450 after ammonium ion-exchange using aqueous solution of NH_4NO_3
MOR-550-NH_4	H–MOR-550 after ammonium ion-exchange using aqueous solution of NH_4NO_3

hydration at room temperature.[52] The ^{27}Al MAS NMR spectrum of NH_4–MOR contains one resonance at around 56 ppm, characteristic of tetrahedral framework aluminum. Upon calcining NH_4–MOR in static air at 450 °C and subsequent exposure to ambient conditions (H–MOR-450), a fraction of aluminum adopts an octahedral geometry, evidenced by the sharp resonance at 0 ppm. There is an additional change in the spectrum of the sample calcined at a higher temperature of 550 °C (H–MOR-550). Besides the presence of octahedrally coordinated aluminum, the tetrahedral feature at 56 ppm has a broad shoulder stretching to lower chemical shifts. This broadening is not present in the spectrum of NH_4–MOR and is barely discernible in that of H–MOR-450. Octahedrally coordinated aluminum represents 11% of the total aluminum content in H–MOR-550 and 10% of the total aluminum content in H–MOR-450.

Octahedrally coordinated aluminum in mordenite, which is characterized by a narrow resonance at 0 ppm by ^{27}Al MAS NMR, can be forced back into the typical framework tetrahedral geometry on back-exchanging the zeolite to its ammonium form.[30] This phenomenon of reversible octahedral–tetrahedral aluminum coordination was first observed for zeolite BEA,[46] and later confirmed[40] and generalized for other zeolites.[15,31,48,50,53] Likewise, we observe that the octahedrally coordinated species in both, H–MOR-450 and H–MOR-550, can be forced back into a tetrahedral environment on ammonium-exchange (Fig. 2). The sharpness of the feature at 0 ppm implies that the electric field gradient surrounding this aluminum atom is small and therefore suggests a high symmetry.

The conversion of tetrahedrally coordinated framework aluminum to an octahedral coordination is driven by the adsorption of water through hydrolysis reactions.[50,54,55] The original proposal for the octahedral framework-associated species was that the aluminum is connected to the framework *via* four oxygen atoms with a water molecule and a hydronium ion being the two other coordinations.[46] However, theoretical work shows that hydrolysis of Si–O and Al–O bonds readily occur and a fourfold coordination to the framework is

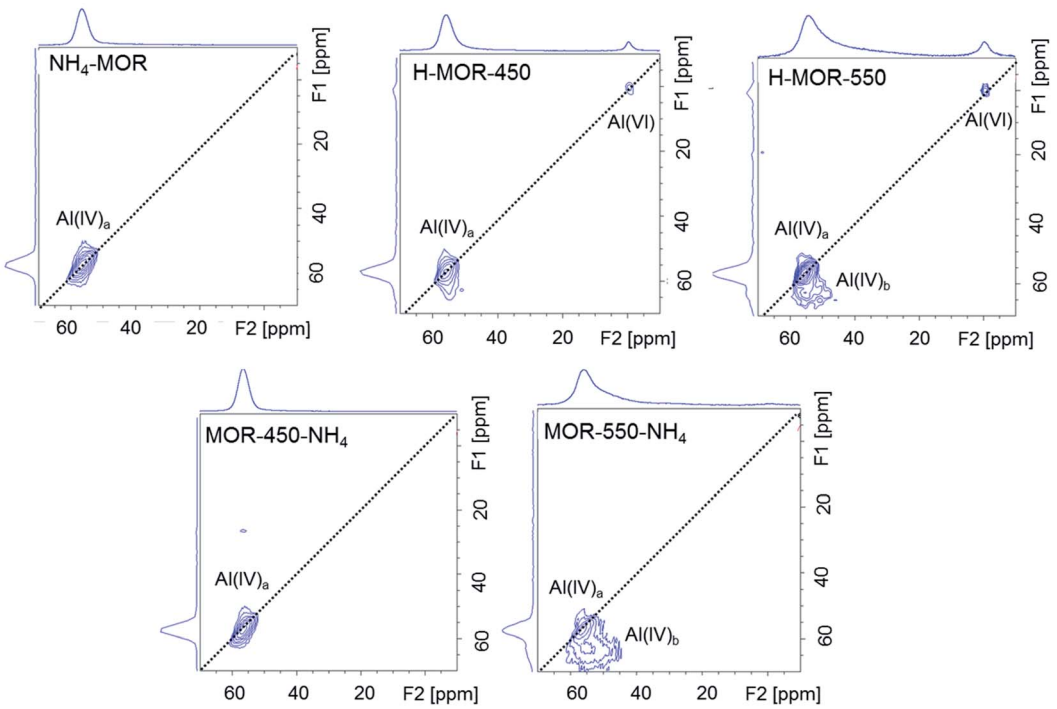

Fig. 3 ^{27}Al MQMAS NMR spectra measured under ambient conditions for NH_4–MOR, H–MOR-450, H–MOR-550, MOR-450-NH_4 and MOR-550-NH_4. The F1 projection shows a purely isotropic dimension and the F2 projection depicts the corresponding ^{27}Al MAS NMR spectrum, which is acquired in a separate experiment.

unlikely.[42] Despite the lack of certainty about the exact structure, enough experimental evidence has emerged to suggest that such octahedrally coordinated aluminum cannot be trivially dismissed as EFAl.[46–48]

The ^{27}Al MQMAS NMR spectrum of NH_4–MOR shows a single feature assigned to tetrahedral framework aluminum (Fig. 3). The spectrum of H–MOR-550 shows two types of tetrahedrally coordinated aluminum species, one type of octahedrally coordinated species and no penta-coordinated aluminum. The ^{27}Al MQMAS spectrum demonstrates that the two types of tetrahedral species have different anisotropy. Tetrahedrally coordinated framework aluminum denoted as Al(IV)$_a$ hugs onto the F1 = F2 diagonal pointing to a very low anisotropic quadrupolar interaction. In contrast, the significant quadrupolar interaction for the Al(IV)$_b$ sites is evidenced by the broad contours parallel to the F2 dimension. The absence of penta-coordinated aluminum is in line with the findings from Chen *et al.*, who have previously detected five-coordinated aluminum in mordenite only upon calcination at temperatures in excess of 650 °C.[56] The fraction of Al(IV)$_b$ is a function of calcination temperature. Such species is barely detectable in the spectrum of H–MOR-450. However, this sample does contain a substantial amount of octahedrally coordinated aluminum, suggesting that the Al(IV)$_b$ species is not a precursor to the Al(VI) sites.

Fig. 3 shows that the ^{27}Al MQMAS NMR spectrum of MOR-450-NH_4 is very similar to that of NH_4–MOR, but the same observation does not hold for MOR-550-NH_4. In the spectrum of the latter, the resonance of the Al(VI) species disappears and that of Al(IV)$_a$ reappears but that of Al(IV)$_b$ species continues to be present. The population of distorted tetrahedral Al(IV)$_b$ sites is an important point of difference between the spectra of MOR-550-NH_4 and NH_4–MOR. Since the Al(IV)$_b$ sites are only formed at a calcination temperature of 550 °C, these aluminum species most likely represent irreversible thermal damage inflicted on the zeolite framework, preventing their transformation back into a framework T-site, unlike the framework-associated octahedrally coordinated aluminum.

The phenomenon of reversible tetrahedral–octahedral aluminum coordination in zeolite mordenite can be realized independent of the Si/Al ratio. To illustrate this, we calcined three ammonium–mordenite samples of different Si/Al ratio at 550 °C to obtain the corresponding proton forms (Table S1†). The percentage of octahedrally coordinated aluminum decreases from 13% for zeolite MOR with a Si/Al ratio of 8.8 to 10% for a sample of a higher Si/Al ratio of 19.7. In comparison, up to 19% of aluminum adopts an octahedral coordination in

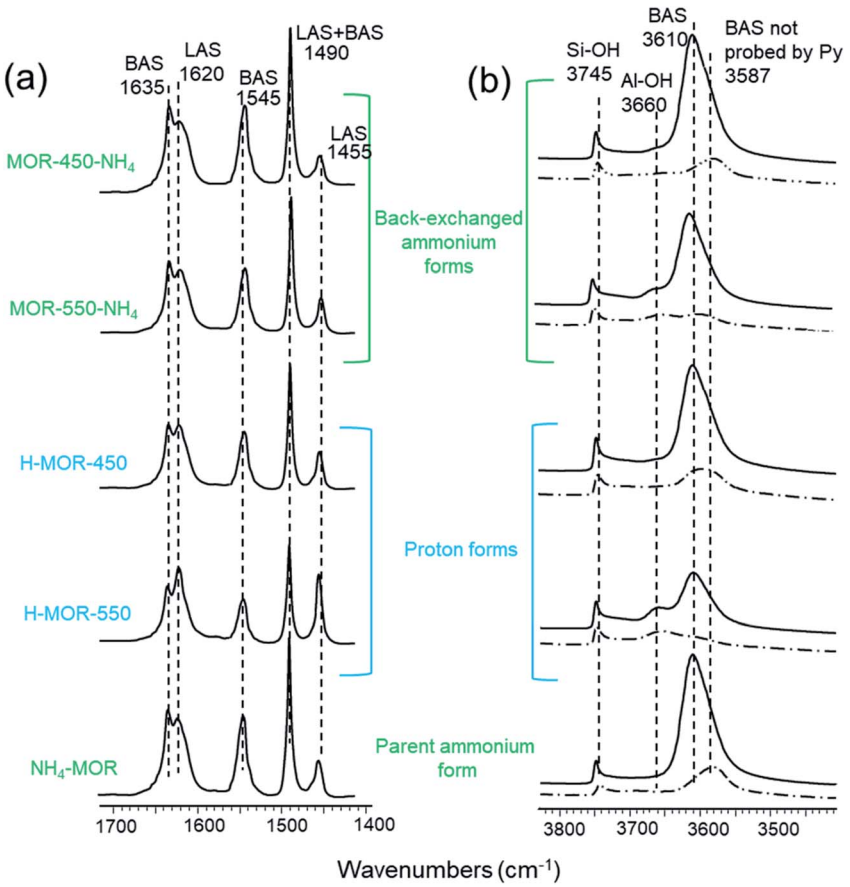

Fig. 4 FTIR spectra of (a) adsorbed pyridine over activated NH_4–MOR, H–MOR-450, H–MOR-550, MOR-450-NH_4 and MOR-550-NH_4; (b) samples activated under vacuum at 450 °C for 4 h (solid line) and after pyridine adsorption–desorption at 150 °C (dashed line) in the OH stretching region. The names of the samples refer to the form of the zeolite prior to heat treatment in the IR setup.

the proton form of zeolite BEA with a Si/Al ratio of 9.[57] When the protonic zeolites are exchanged back into the ammonium form, we observe a quantitative transformation of octahedrally coordinated aluminum into tetrahedral coordination (Table S1†).

Relationship between aluminum coordination and Brønsted–Lewis acidity

Fig. 4a depicts the FTIR spectra of NH_4–MOR, H–MOR-450, H–MOR-550, MOR-450-NH_4 and MOR-550-NH_4 after *in situ* high temperature evacuation and pyridine adsorption–desorption. The names of the samples in the figure refer to the form of the zeolite prior to heat treatment in the IR setup; high temperature activation of the samples under vacuum before pyridine adsorption–desorption converts all the zeolites to the proton form. The absorption features at 1455 and 1620 cm^{-1} in Fig. 4a are assigned to pyridine bound to Lewis acid sites, while those at 1545 and 1635 cm^{-1} correspond to protonated pyridine. Activation of NH_4–MOR under vacuum results in a minor population of Lewis acid sites. In a previous study, we established that framework-associated aluminum in proton-exchanged zeolites adopts an octahedral coordination under ambient conditions and is the precursor for Lewis acid sites.[30] Upon activation, both H–MOR-450 and H–MOR-550 have a lower concentration of Brønsted acid sites (BAS, 1545 cm^{-1}) than NH_4–MOR. Likewise, the spectrum of H–MOR-450 exhibits a larger peak associated with Brønsted acidity (1545 cm^{-1}) and a smaller feature corresponding to Lewis acidity (LAS, 1455 cm^{-1}) than that of H–MOR-550. Therefore, the generation of Lewis acid sites is accompanied by a loss of Brønsted acid sites. In other words, some of the framework aluminum that generate Brønsted acidity convert into framework-associated octahedrally coordinated species, which after dehydration show Lewis acidity. Fig. 4a and Table 2 show that MOR-450-NH_4 and MOR-550-NH_4 have lower Lewis acid and higher Brønsted acid concentrations after *in situ* activation than the corresponding proton forms, H–MOR-450 and H–MOR-550. This observation is consistent with the ^{27}Al NMR results discussed earlier, where aluminum in octahedral coordination in the proton form of mordenite was shown to reinsert into the framework upon converting to the ammonium form (*vide supra*). Consequently, the conversion of the Lewis acid-forming framework-associated aluminum to a typical tetrahedral framework species results in increased Brønsted acidity upon *in situ* activation of the back-exchanged samples. The greater intensity of the peak corresponding to pyridinium ion in the FTIR spectra of the activated back ammonium-exchanged samples duly reflects this.

Fig. 4b illustrates the FTIR spectra of the same samples in the OH stretching region, before and after pyridine adsorption–desorption. The most prominent absorption in the evacuated samples is that at 3610 cm^{-1}, which is attributed to bridging hydroxyl groups (Brønsted acid sites). The feature at 3745 cm^{-1} is the signature for silanols. FTIR spectra of H–MOR-550 and MOR-550-NH_4 (Fig. 4b) show a shoulder at around 3660 cm^{-1}, which is attributed to the presence of Al–OH species.[58] This feature is barely visible in the spectra of NH_4–MOR, H–MOR-450 and MOR-450-NH_4. The peak area associated with Brønsted acid sites decreases in the order NH_4–MOR $\approx$ MOR-450-NH_4 > H–MOR-450 > MOR-550-NH_4 > H–MOR-550 (Table 2). The total Brønsted acidity measured after high temperature *in situ* activation of MOR-450-NH_4 is highly comparable to that of *in situ* activated NH_4–MOR. However, in the case of MOR-550-NH_4, the total Brønsted acidity, while being appreciably higher than in H–MOR-550, is still inferior to that of NH_4–MOR. Therefore, the extent to which Brønsted acid sites are restored depends on the temperature at which the proton form is calcined. A nearly complete retrieval of Brønsted acidity is possible with the zeolite calcined at 450 °C, but not with samples calcined at higher temperatures. The presence of irreversibly formed Al–OH groups in MOR-550-NH_4 results in the total Brønsted acidity being inferior to that of NH_4–MOR (Table 2).

After adsorption of pyridine at 150 °C followed by desorption at the same temperature, the spectrum of activated NH_4–MOR shows a feature centered at approximately 3587 cm^{-1} in the OH-stretching region (Fig. 4b). This corresponds to the fraction of Brønsted acid sites that are not probed by pyridine. The side-pockets in mordenite present accessibility limitations for sterically bulky molecules. While pyridine can access Brønsted acid sites in the main channel in a pristine mordenite sample, it cannot probe bridging OH groups located in the side-pockets.[59–61] The above-mentioned OH-stretch frequency at 3587 cm^{-1} is representative of such inaccessible Brønsted acid sites. This feature continues to be present in the spectrum of H–MOR-450, but is barely observed in the spectrum of H–MOR-550 (Fig. 4b). The disappearance of this feature suggests that only a small number of bridging hydroxyl groups remain in the side-pockets of the H–MOR-550 sample and that nearly all bridging hydroxyl groups can be accessed by pyridine.

Using carbon monoxide as a probe molecule enables the distinction of Lewis acid sites in terms of their coordination number. Assuming the assignment of IR signatures from published literature, the interaction of carbon monoxide with three- and five-coordinated Lewis acidic aluminum result in FTIR absorption bands at 2224 cm^{-1} and 2198 cm^{-1} respectively.[62–64] Three-coordinated Lewis acid sites are typically found in mordenite zeolites of both high and low aluminum content, but

Table 2 Analysis of total Brønsted (BAS) and Lewis acidity (LAS) in the different mordenite samples

Sample	BAS peak area[a] [a.u.]	LAS peak area as assessed using pyridine[b] [a.u.]	LAS peak area as assessed using carbon monoxide[c] [a.u.]
NH_4–MOR	52	3.9	1.2
H–MOR-450	41	4.1	1.6
H–MOR-550	26	6.5	1.8
MOR-450-NH_4	49	3.5	1.2
MOR-550-NH_4	37	3.6	1.1

[a] Computed by integration of the peak at 3609 cm^{-1} in the activated sample. [b] Computed by integration of the peak at 1455 cm^{-1} in the pyridine-adsorbed sample. [c] Computed by integration of the peaks at 2224 cm^{-1} and 2198 cm^{-1} in the CO-adsorbed sample. The relative error for all numbers listed in the table is ±5%.

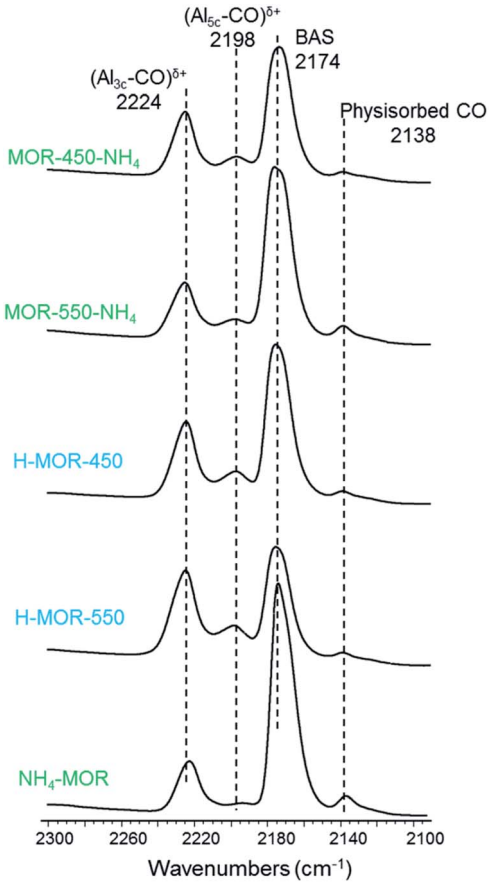

Fig. 5 FTIR spectra of adsorbed carbon monoxide over activated parent ammonium form NH_4–MOR, H–MOR-450, H–MOR-550, MOR-450-NH_4 and MOR-550-NH_4. The names of the samples refer to the form of the zeolite prior to heat treatment in the IR setup.

five-coordinated aluminum species are detected in appreciable amounts only in samples of low Si/Al ratio.[30] Fig. 5 reveals that a major portion of Lewis acid sites after activation of each sample is three-coordinated. Calcining NH_4–MOR *in situ* under vacuum results in an almost ideal proton form with a low contribution of Lewis acid sites. While this sample is largely devoid of five-coordinated Lewis acid sites, such sites are present in non-negligible amounts in the other samples.

The findings presented in this section constitute an important conceptual advance in the relationship between aluminum coordination and Brønsted–Lewis acidity in zeolites (Scheme 1). Framework aluminum adopts a tetrahedral geometry in the ammonium form of the zeolite. *In situ* activation of such sample yields Brønsted acid sites through ammonia removal. On the other hand, when NH_4–MOR is calcined in static air and exposed to ambient conditions, a fraction of the aluminum described as being associated to the framework adopts octahedral geometry. Upon high-temperature activation, this aluminum species has Lewis acidic character. When the acidic form of the zeolite is back-exchanged into the ammonium form, the framework-associated aluminum reverts to a tetrahedral geometry. *In situ* activation of such a back-exchanged sample shows low Lewis and high Brønsted acid concentration.

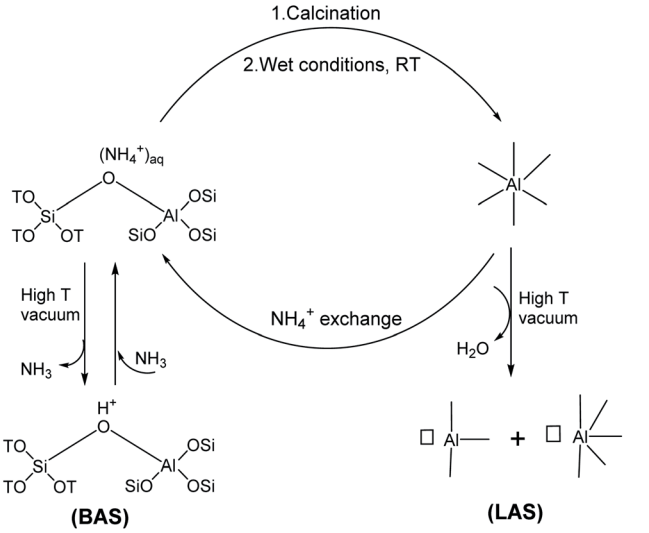

Scheme 1 Reversible tetrahedral–octahedral coordination exhibited by framework-associated aluminum and its impact on Brønsted and Lewis acidity.

Therefore, the property of reversible tetrahedral–octahedral coordination exhibited by framework-associated aluminum facilitates the indirect switching between Brønsted and Lewis acidity (Scheme 1). While the switch in acidity was experimentally observed herein with mordenite, we believe that this can be extended to zeolite topologies that allow the formation of octahedrally coordinated framework-associated aluminum, which have been observed in a range of different zeolites, including BEA[46] and zeolite Y.[50]

Location of framework-associated aluminum in the pore system of mordenite

The Lewis acid content detected with pyridine as the probe molecule in H–MOR-450 is only marginally higher than that in activated NH_4–MOR (Table 2). However, there is a large difference in the Lewis acid site concentration between H–MOR-450 and H–MOR-550. From ^{27}Al MAS NMR, we know that the fraction of Al(VI) in these acidic zeolites are not substantially different (*vide supra*). Therefore, the large difference in the intensity of the peak at 1455 cm^{-1} for these two zeolites (Fig. 4a, Table 2) might not reflect such a quantitative difference in acid site density, but instead could be caused by differences in accessibility of the Lewis acid sites for pyridine. Being a much smaller molecule, carbon monoxide can probe all acid sites in mordenite, including the ones located deep in the side-pockets. From Fig. 5 and Table 2, we infer that the Lewis acid site concentration detected with carbon monoxide in H–MOR-450 and H–MOR-550 differ minimally, while being higher than that observed in *in situ* activated NH_4–MOR. This suggests that the much lower Lewis acid content, as measured with pyridine in H–MOR-450 compared to H–MOR-550, is due to differences in acid site accessibility for pyridine. Fig. 4b corroborates this hypothesis from the context of Brønsted acid site accessibility. While a substantial portion of bridging hydroxyl groups in

H–MOR-450 remain inaccessible to pyridine, nearly all Brønsted acid sites can be probed in H–MOR-550 (dashed lines, Fig. 4b). Previous studies on zeolite mordenite of a comparable Si/Al ratio suggested that pyridine can access a part of Brønsted acid sites in the side-pockets in the proton form calcined at 550 °C, which is not the case with the parent ammonium form.[59,60,65] Based on these findings, it appears that Lewis acid sites originating from framework-associated aluminum tend to be localized more in the side pockets than in the main channel of mordenite. This would explain why the Lewis acidity measured with pyridine in H–MOR-450, wherein pyridine has considerable accessibility limitations in the side-pockets, is much lower than the acidity measured in H–MOR-550, wherein these restrictions are more relaxed. And notably, the use of carbon monoxide reveals a smaller difference in Lewis acid content between these two samples.

The Al–OH groups, which are present in H–MOR-550 and characterized by the IR band at 3660 cm^{-1}, do not engage in a Lewis acidic interaction with pyridine. The corresponding back-exchanged sample, MOR-550-NH_4, continues to have appreciable amounts of Al–OH moieties (Fig. 4b), but shows Lewis acidity that is comparable to activated NH_4–MOR and MOR-450-NH_4 (Table 2), neither of which show signatures for Al–OH. The Al–OH groups are also not Brønsted acidic, since the signature for these species in the OH stretching region remains largely unperturbed after pyridine adsorption (dashed lines, Fig. 4b). The low Lewis acid content in MOR-550-NH_4, as detected by pyridine, is unlikely to be caused by accessibility limitations as most of the Brønsted acid sites in this sample can be accessed by pyridine (dashed line, Fig. 4b). Consequently, the low Lewis acid content of MOR-550-NH_4 is truly reflective of the transformation of Lewis acid-forming framework-associated aluminum to tetrahedral framework aluminum, which is not Lewis acidic. This observation is further validated by measurements of Lewis acidity using carbon monoxide (Table 2).

While the concept of certain aluminum species exhibiting reversible tetrahedral-octahedral coordination has been reported in the past, we show that Lewis acid sites originating from framework-associated aluminum has preferential site occupancy in zeolites; in the case of mordenite, the side-pockets are more favored to host these sites than the main channel. This insight can have far-reaching implications for the rational synthesis of Lewis acid sites in zeolites by virtue of controlling aluminum distribution.[66] Furthermore, such information on site specificity can aid in the engineering of improved catalysts, as realized in the case of Brønsted acid-catalyzed carbonylation.[67] While the distribution of Brønsted acid sites can be assessed using ^{1}H DQMAS NMR of acetonitrile-d_3 adsorbed over mordenite, catalytic activity in the carbonylation of dimethyl ether correlates with the number of acidic protons in the side-pockets.[68,69] Analogous to these findings on the specificity of Brønsted acid sites in carbonylation reactions, knowledge on the site specificity of Lewis acid sites in zeolites will enhance the understanding of their role(s) in catalytic applications.

As is generally observed with different zeolite types, the amount of octahedrally coordinated framework-associated aluminum in the proton form of mordenite decreases with increasing Si/Al ratio.[30] The negligible amount of octahedrally coordinated aluminum in the proton form of Si-rich zeolites suggests that isolated aluminum atoms do not undergo this phenomenon, and instead, two or more aluminum atoms in close proximity might be needed for the generation of octahedral framework-associated species. Based on the FTIR results presented herein, the side-pockets in mordenite can be envisioned to provide a more favorable environment in terms of proximal aluminum location for the generation and stabilization of octahedral framework-associated aluminum. In this context, it is worth noting that the relatively stronger acidity of Brønsted acid sites in the side-pockets compared to those in the main channel of mordenite is assigned to the stronger confinement effect imposed by the zeolite framework.[68]

Al–OH groups and its relation to distorted tetrahedrally coordinated aluminum

The FTIR spectroscopic signature at around 3660 cm^{-1} for Al–OH groups correlates with the signature for distorted tetrahedrally coordinated aluminum on the ^{27}Al MQMAS NMR. Fig. 4b shows that Al–OH species is virtually non-existent in the spectra of NH_4–MOR and H–MOR-450, but present in substantial amounts in the spectrum of H–MOR-550. Stacking this against the corresponding ^{27}Al MQMAS NMR spectra (Fig. 3) reveals that Al–OH groups are linked to the distorted tetrahedral sites ($Al(IV)_b$). The same interpretation can also be drawn from the back-exchanged ammonium samples. MOR-450-NH_4 has a negligible population of distorted tetrahedral sites, as evidenced by ^{27}Al MQMAS NMR (Fig. 3) and correspondingly, no pronounced feature for Al–OH groups in the FTIR spectrum (Fig. 4b). MOR-550-NH_4 has a far more substantial number of distorted tetrahedral sites on the ^{27}Al MQMAS NMR and correspondingly, a distinct feature for Al–OH groups in the FTIR spectrum. Consequently, the generation of the Al–OH species upon calcination at high temperatures corresponds to a different aluminum species than the framework-associated aluminum that changes coordination. H–MOR-450 is exemplar of this hypothesis as it has appreciable amounts of octahedrally coordinated aluminum but barely any distorted tetrahedral aluminum on the ^{27}Al MQMAS NMR (Fig. 3) or signature for Al–OH groups in the FTIR spectrum (Fig. 4b).

Therefore, octahedrally coordinated aluminum in mordenite, Al(VI), which is characterized by the narrow ^{27}Al signal at around 0 ppm under hydrated conditions - and which shows Lewis acidic behavior after dehydration – is able to revert into a framework site. However, distorted tetrahedrally coordinated aluminum, $Al(IV)_b$, which has one or more OH coordinations and is generated by calcination at a higher temperature, behaves differently and does not change coordination upon ammonium exchange. While substantial amounts of octahedrally coordinated aluminum is present under ambient conditions in H–MOR-450 (Fig. 2), the accessibility limitations for pyridine in this sample is comparable to that in NH_4–MOR (Fig. 4b). Based on this observation and on the FTIR line shapes of H–MOR-550 and MOR-550-NH_4 after pyridine adsorption (Fig. 4b), it appears that it is the distorted tetrahedral sites, and

not the octahedrally coordinated species, that modify accessibility for pyridine to acid sites in the side-pockets.

Evolution of aluminum structure with conditions in mordenite

Scheme S1† summarizes the key findings from this study and presents the evolution of aluminum structure in zeolite mordenite as a function of conditions. The NMR and FTIR spectroscopic signatures used for the assignment of different species are listed in a table as part of Scheme S1.† We further indicate the nature of each species, as likely being/originating from framework, extra-framework or framework-associated aluminum. Calcining the ammonium form of mordenite at 450 °C in static air and subsequent exposure of the sample to ambient conditions yields the proton form of the zeolite (H_MOR_wet in Scheme S1†) with aluminum in two different geometries: tetrahedral framework aluminum ($Al(IV)_a$) and octahedrally coordinated framework-associated aluminum ($Al(VI)$). The zeolite is devoid of penta-coordinated and distorted tetrahedral aluminum moieties. Evacuating H_MOR_wet at elevated temperature converts the octahedrally coordinated aluminum species into primarily three-coordinated and some five-coordinated Lewis acidic species (H_MOR_activated in Scheme S1†) that are preferentially localized in the side-pockets of mordenite.[30] Upon ammonium exchange of the H_MOR_wet sample, the coordination environment of aluminum in the zeolite reverts to being exclusively tetrahedral (H_MOR_NH_4 in Scheme S1†), as present in the parent NH_4_MOR. While such a change in aluminum coordination from octahedral to tetrahedral has been observed with several zeolite topologies, an elaborate mechanism on how ammonium ion-exchange, or equivalently ammonia treatment, facilitates this transformation is yet to be deduced and should be a key research direction to be explored in the future.[47,55] Evacuating H_MOR_NH_4 under vacuum at high temperature shows greater Brønsted acidity that in the preceding proton form. This is because the conversion of octahedrally coordinated aluminum to a tetrahedral geometry on ammonium exchange restores the typical tetrahedrally coordinated framework aluminum, which yield bridging hydroxyl groups upon ammonia removal. The evolution of aluminum structure on calcining the ammonium form of the zeolite at a higher temperature of 550 °C in static air is largely similar to the evolution observed with the sample calcined at a lower temperature of 450 °C but for one important difference. The treatment at the higher temperature generates distorted tetrahedral aluminum sites (H_MOR_highT_wet in Scheme S1†), which result in anisotropic broadening in the ^{27}Al MAS NMR spectrum of this proton form. In the FTIR spectrum, the Al–OH species are characterized by an absorption at 3660 cm^{-1} in the OH stretching region and they do not interact with pyridine. While ammonium ion-exchange renders it possible to convert all octahedrally coordinated framework-associated aluminum into tetrahedral coordination, the distorted tetrahedral aluminum sites do not revert to the pristine tetrahedral framework coordination (H_MOR_highT_NH_4 in Scheme S1†).

Conclusions

Proton forms of zeolite mordenite, obtained by the calcination of the parent ammonium form in wet static air, possess framework-associated octahedrally coordinated aluminum under ambient conditions. After high temperature activation of such sample, the framework-associated aluminum shows Lewis acidic property. The changes in aluminum coordination and conversion of Brønsted into Lewis acidity are partially reversible. Exchanging the proton form back into the ammonium form converts octahedrally coordinated aluminum back into a framework tetrahedral coordination, with the bridging hydroxyl groups being formed upon ammonia removal. The degree of retrieval of Brønsted acidity is a function of the calcination temperature. Higher calcination temperature yields a distorted tetrahedrally coordinated aluminum species that is irreversibly formed and is characterized by a high anisotropy of chemical shift. This species contributes to the IR feature at 3660 cm^{-1} in the OH-stretching region, assigned to Al–OH moieties. The presence of these Al–OH species modifies pyridine accessibility to the acid sites in the side-pockets of mordenite. The attribute of framework-associated aluminum to undergo reversible transformation in coordination from tetrahedral to octahedral enables the possibility to switch between Brønsted and Lewis acidity. Aluminum in the side-pockets in mordenite are more prone to show such behavior. Therefore, Lewis acid sites formed from framework-associated aluminum are found to have a preferential site occupancy in the pore structure of mordenite. These observations are fundamentally different to the largely researched Lewis acidic extra-framework aluminum and could enable a paradigm shift in the rational design of Lewis acid sites in zeolites.

Conflicts of interest

There are no conflicts of interest to declare.

References

1 C. Marcilly, *J. Catal.*, 2003, **216**, 47–62.
2 G. Sartori and R. Maggi, *Chem. Rev.*, 2006, **106**, 1077–1104.
3 W. O. Haag, R. M. Lago and P. B. Weisz, *Nature*, 1984, **309**, 589.
4 W. F. Hölderich and H. Van Bekkum, in *Studies in Surface Science and Catalysis*, Elsevier, 1991, vol. 58, pp. 631–726.
5 E. T. C. Vogt and B. M. Weckhuysen, *Chem. Soc. Rev.*, 2015, **44**, 7342–7370.
6 K. M. Minachev, V. I. Garanin, V. V. Kharlamov, T. A. Isakova and E. E. Senderov, *Russ. Chem. Bull.*, 1969, **18**, 1611–1615.
7 I. E. Maxwell, *Catal. Today*, 1987, **1**, 385–413.
8 E. Taarning, C. M. Osmundsen, X. Yang, B. Voss, S. I. Andersen and C. H. Christensen, *Energy Environ. Sci.*, 2011, **4**, 793–804.
9 H. Y. Luo, J. D. Lewis and Y. Román-Leshkov, *Annu. Rev. Chem. Biomol. Eng.*, 2016, **7**, 663–692.

10 P. P. Pescarmona, K. P. F. Janssen, C. Delaet, C. Stroobants, K. Houthoofd, A. Philippaerts, C. De Jonghe, J. S. Paul, P. A. Jacobs and B. F. Sels, *Green Chem.*, 2010, **12**, 1083–1089.
11 P. Lanzafame, D. M. Temi, S. Perathoner, A. N. Spadaro and G. Centi, *Catal. Today*, 2012, **179**, 178–184.
12 M. Maache, A. Janin, J. C. Lavalley, J. F. Joly and E. Benazzi, *Zeolites*, 1993, **13**, 419–426.
13 C. A. Emeis, *J. Catal.*, 1993, **141**, 347–354.
14 S. M. Maier, A. Jentys and J. A. Lercher, *J. Phys. Chem. C*, 2011, **115**, 8005–8013.
15 B. Gil, S. I. Zones, S.-J. Hwang, M. Bejblová and J. Čejka, *J. Phys. Chem. C*, 2008, **112**, 2997–3007.
16 M. Boronat and A. Corma, *ACS Catal.*, 2019, **9**, 1539–1548.
17 N. S. Nesterenko, F. Thibault-Starzyk, V. Montouillout, V. V. Yuschenko, C. Fernandez, J. P. Gilson, F. Fajula and I. I. Ivanova, *Microporous Mesoporous Mater.*, 2004, **71**, 157–166.
18 L. Bui, H. Luo, W. R. Gunther and Y. Román-Leshkov, *Angew. Chem., Int. Ed.*, 2013, **52**, 8022–8025.
19 P. Y. Dapsens, C. Mondelli and J. Pérez-Ramírez, *Chem. Soc. Rev.*, 2015, **44**, 7025–7043.
20 T. D. Swift, H. Nguyen, Z. Erdman, J. S. Kruger, V. Nikolakis and D. G. Vlachos, *J. Catal.*, 2016, **333**, 149–161.
21 V. V. Ordomsky, V. L. Sushkevich, J. C. Schouten, J. Van Der Schaaf and T. A. Nijhuis, *J. Catal.*, 2013, **300**, 37–46.
22 S. Suganuma, T. Hisazumi, K. Taruya, E. Tsuji and N. Katada, *ChemistrySelect*, 2017, **2**, 5524–5531.
23 M. A. Bañares, J. H. Cardoso, G. J. Hutchings, J. M. C. Bueno and J. L. G. Fierro, *Catal. Lett.*, 1998, **56**, 149–153.
24 B. Wichterlová, Z. Tvarůžková, Z. Sobalík and P. Sarv, *Microporous Mesoporous Mater.*, 1998, **24**, 223–233.
25 X. Pu, N.-w. Liu and L. Shi, *Microporous Mesoporous Mater.*, 2015, **201**, 17–23.
26 J. Brus, L. Kobera, W. Schoefberger, M. Urbanová, P. Klein, P. Sazama, E. Tabor, S. Sklenak, A. V. Fishchuk and J. Dědeček, *Angew. Chem., Int. Ed.*, 2015, **54**, 541–545.
27 T. K. Phung and G. Busca, *Appl. Catal., A*, 2015, **504**, 151–157.
28 G. Busca, *Microporous Mesoporous Mater.*, 2017, **254**, 3–16.
29 X. Yi, K. Liu, W. Chen, J. Li, S. Xu, C. Li, Y. Xiao, H. Liu, X. Guo and S.-B. Liu, *J. Am. Chem. Soc.*, 2018, **140**, 10764–10774.
30 M. Ravi, V. L. Sushkevich and J. A. van Bokhoven, *J. Phys. Chem. C*, 2019, **123**, 15139–15144.
31 G. L. Woolery, G. H. Kuehl, H. C. Timken, A. W. Chester and J. C. Vartuli, *Zeolites*, 1997, **19**, 288–296.
32 P. A. Jacobs and H. K. Beyer, *J. Phys. Chem.*, 1979, **83**, 1174–1177.
33 U. Lohse, E. Löffler, M. Hunger, J. Stöckner and V. Patzelova, *Zeolites*, 1987, **7**, 11–13.
34 X. Yi, K. Liu, W. Chen, J. Li, S. Xu, C. Li, Y. Xiao, H. Liu, X. Guo, S.-B. Liu and A. Zheng, *J. Am. Chem. Soc.*, 2018, **140**, 10764–10774.
35 M. Ravi, V. L. Sushkevich and J. A. van Bokhoven, *Nat. Mater.*, 2020, **19**, 1047–1056.
36 Z. Yu, S. Li, Q. Wang, A. Zheng, X. Jun, L. Chen and F. Deng, *J. Phys. Chem. C*, 2011, **115**, 22320–22327.
37 S. Li, A. Zheng, Y. Su, H. Fang, W. Shen, Z. Yu, L. Chen and F. Deng, *Phys. Chem. Chem. Phys.*, 2010, **12**, 3895–3903.
38 R. A. Beyerlein, C. Choi-Feng, J. B. Hall, B. J. Huggins and G. J. Ray, *Top. Catal.*, 1997, **4**, 27–42.
39 V. L. Zholobenko, L. M. Kustov, V. B. Kazansky, E. Loeffler, U. Lohser, C. Peuker and G. Oehlmann, *Zeolites*, 1990, **10**, 304–306.
40 J. A. van Bokhoven, D. C. Koningsberger, P. Kunkeler, H. Van Bekkum and A. P. M. Kentgens, *J. Am. Chem. Soc.*, 2000, **122**, 12842–12847.
41 G. Catana, D. Baetens, T. Mommaerts, R. A. Schoonheydt and B. M. Weckhuysen, *J. Phys. Chem. B*, 2001, **105**, 4904–4911.
42 Z. Yu, A. Zheng, Q. Wang, L. Chen, J. Xu, J. P. Amoureux and F. Deng, *Angew. Chem., Int. Ed.*, 2010, **49**, 8657–8661.
43 S. Xin, Q. Wang, J. Xu, Y. Chu, P. Wang, N. Feng, G. Qi, J. Trébosc, O. Lafon and W. Fan, *Chem. Sci.*, 2019, **10**, 10159–10169.
44 T. T. Le, A. Chawla and J. D. Rimer, *J. Catal.*, 2020, **391**, 56–68.
45 K. Chen, S. Horstmeier, V. T. Nguyen, B. Wang, S. P. Crossley, T. Pham, Z. Gan, I. Hung and J. L. White, *J. Am. Chem. Soc.*, 2020, **142**, 7514–7523.
46 E. Bourgeat-Lami, P. Massiani, F. Di Renzo, P. Espiau, F. Fajula and T. Des Courières, *Appl. Catal.*, 1991, **72**, 139–152.
47 A. Omegna, J. A. van Bokhoven and R. Prins, *J. Phys. Chem. B*, 2003, **107**, 8854–8860.
48 J. A. van Bokhoven, A. M. J. Van der Eerden and D. C. Koningsberger, *J. Am. Chem. Soc.*, 2003, **125**, 7435–7442.
49 D. Ma, F. Deng, R. Fu, X. Han and X. Bao, *J. Phys. Chem. B*, 2001, **105**, 1770–1779.
50 B. H. Wouters, T. H. Chen and P. J. Grobet, *J. Am. Chem. Soc.*, 1998, **120**, 11419–11425.
51 J. A. van Bokhoven, *Phys. Scr.*, 2005, **2005**, 76–79.
52 Z. Zhao, S. Xu, M. Y. Hu, X. Bao, C. H. F. Peden and J. Hu, *J. Phys. Chem. C*, 2014, **119**, 1410–1417.
53 P. J. Kunkeler, B. J. Zuurdeeg, J. C. Van der Waal, J. A. van Bokhoven, D. C. Koningsberger and H. Van Bekkum, *J. Catal.*, 1998, **180**, 234–244.
54 L. C. De Ménorval, W. Buckermann, F. Figueras and F. Fajula, *J. Phys. Chem.*, 1996, **100**, 465–467.
55 I. J. Drake, Y. Zhang, M. K. Gilles, C. N. Teris Liu, P. Nachimuthu, R. C. C. Perera, H. Wakita and A. T. Bell, *J. Phys. Chem. B*, 2006, **110**, 11665–11676.
56 T. H. Chen, B. H. Wouters and P. J. Grobet, *Eur. J. Inorg. Chem.*, 2000, **2000**, 281–285.
57 A. Abraham, S.-H. Lee, C.-H. Shin, S. B. Hong, R. Prins and J. A. van Bokhoven, *Phys. Chem. Chem. Phys.*, 2004, **6**, 3031–3036.
58 I. Kiricsi, C. Flego, G. Pazzuconi, W. O. Parker Jr, R. Millini, C. Perego and G. Bellussi, *J. Phys. Chem.*, 1994, **98**, 4627–4634.
59 J. Datka, B. Gil and A. Kubacka, *Zeolites*, 1997, **18**, 245–249.

60 F. Moreau, P. Ayrault, N. S. Gnep, S. Lacombe, E. Merlen and M. Guisnet, *Microporous Mesoporous Mater.*, 2002, **51**, 211–221.
61 X. Li, R. Prins and J. A. van Bokhoven, *J. Catal.*, 2009, **262**, 257–265.
62 L. M. Kustov, V. B. Kazanskii, S. Beran, L. Kubelkova and P. Jiru, *J. Phys. Chem.*, 1987, **91**, 5247–5251.
63 S. Bordiga, E. E. Platero, C. O. Areán, C. Lamberti and A. Zecchina, *J. Catal.*, 1992, **137**, 179–185.
64 F. Wakabayashi, J. N. Kondo, K. Domen and C. Hirose, *J. Phys. Chem.*, 1995, **99**, 10573–10580.
65 S. Grundner, M. A. C. Markovits, G. Li, M. Tromp, E. A. Pidko, E. J. M. Hensen, A. Jentys, M. Sanchez-Sanchez and J. A. Lercher, *Nat. Commun.*, 2015, **6**, 7546.
66 J. Dědeček, E. Tabor and S. Sklenak, *ChemSusChem*, 2019, **12**, 556–576.
67 A. Bhan, A. D. Allian, G. J. Sunley, D. J. Law and E. Iglesia, *J. Am. Chem. Soc.*, 2007, **129**, 4919–4924.
68 X. Yi, Y. Xiao, G. Li, Z. Liu, W. Chen, S.-B. Liu and A. Zheng, *Chem. Mater.*, 2020, **32**, 1332–1342.
69 Z. Liu, X. Yi, G. Wang, X. Tang, G. Li, L. Huang and A. Zheng, *J. Catal.*, 2019, **369**, 335–344.